Efficient Aquatic Locomotion Using Elastic Propulsors With Hybrid Actuation

Ersan Demirer, Oluwafikayo A. Oshinowo, Alexander Alexeev

George W. Woodruff School of Mechanical Engineering, Georgia Institute of Technology

(Received xx; revised xx; accepted xx)

Using computational modeling, we probe the hydrodynamics of a bio-inspired elastic propulsor with hybrid actuation that oscillates at resonance in a Newtonian fluid. The propulsor is actuated by a heaving motion at the base and by an internal bending moment distributed along the propulsor length. The simulations reveal that by tuning the phase difference between the external and internal actuation, the propulsor thrust and free swimming velocity can be regulated in a wide range while maintaining high efficiency. Furthermore, the hybrid propulsor outperforms propulsors with either of the actuation methods. The enhanced performance is associated with the emerging bending pattern maintaining large tip displacement with reduced center of mass displacement. The results are useful for developing highly efficient robotic swimmers utilizing smart materials as propulsors with simplified design and operation.

1. Introduction

The pursuit of more effective means of aquatic locomotion has compelled researchers and engineers to tackle the fluid-structure interaction problem of fish swimming (Chen *et al.* 2009; Combes & Daniel 2001; Liu & Aono 2009; Kolomenskiy *et al.* 2011; Alben *et al.* 2012). While current man-made designs generally rely on rigid propulsors to move through a fluid, nature widely harnesses elasticity for aquatic locomotion (McHenry *et al.* 1995; Jayne & Lauder 1995; Lauder & Tytell 2005; Fish & Lauder 2006). For instance, fish use their muscles to actively change the shape and stiffness of their bodies in order to swim and maneuver (Wardle *et al.* 1995; Ramananarivo *et al.* 2013; Pabst 2015). Fish hydrodynamic performance is intrinsically characterized by the two-way coupling between the deformation of the fish body and the fluid flow. This complex interplay between solid and fluid motion enables fish to yield unmatched swimming velocities, maneuverability, and efficiencies.

Multiple experimental studies explored bio-inspired designs of varying complexity as prototypes for underwater swimmers (Yu *et al.* 2004; Hu *et al.* 2006; Philen & Neu 2011; Marras & Porfiri 2012; Kopman *et al.* 2015). The earliest designs of robotic fish used complex networks of strings and servomotors to replicate the tail motion typically encountered in carangiform swimming modes (Triantafyllou & Triantafyllou 1995; Anderson *et al.* 1998). More recent designs include a series of linked sections coupled to actuators (Flammang & Lauder 2009; Esposito *et al.* 2012; Su *et al.* 2014; Lauder & Tangorra 2015). These locomotion approaches share a common actuation method relying on a form of heaving or pitching motion imposed at the propulsor base. We refer to this method of actuation as the external actuation. Numerous experimental and numerical studies also explored the hydrodynamics of propulsors with a combination of heaving and pitching actuation. For instance, Piñeirua *et al.* (2017), Smits (2019), Van Buren *et al.* (2019) and Quinn *et al.* (2015) investigated the impact of introducing a phase lag between a heaving and pitching actuation. The authors showed that the phase lag is a critical

parameter to maximize the efficiency of the propulsor. Nevertheless, such actuation requires a high level of control of the base motion to enable complex multi-dimensional biomimetic propulsion imposing constraints in terms of propulsor implementation and cost.

Research shows that the elasticity plays a critical role in bio-mimetic locomotion. Using experiments and modeling, Alben *et al.* (2012) demonstrated the existence of resonance peaks in the free swimming velocity of an elastic oscillating plate. The model predicted that the plate velocity is proportional to the plate length to the power of $-1/3$ and plate flexibility to the power of $2/15$. Dai *et al.* (2012) showed that an elastic plate generates significantly more thrust than a rigid plate at the same Strouhal number. Using experiments, Quinn *et al.* (2014) demonstrated the resonance peaks in free swimming velocity occur for discrete values of the effective flexibility defined as a ratio of the added mass and bending forces. Hoover *et al.* (2018) further confirmed these findings with three-dimensional simulations of free swimming flexible plates. Yeh & Alexeev (2014) used fully-coupled three-dimensional simulations to show that elastic propulsors could be operated at a regime of maximum propulsion near the first natural frequency or maximum efficiency away from the resonance.

Recent progress in smart materials allows to overcome certain shortcomings and limitations in designing biomimetic propulsors (Wang *et al.* 2008; Chen *et al.* 2009, 2011; Chu *et al.* 2012). Among different smart materials, internally actuated macro-fiber composites (MFCs) offer a balance between actuation control and deformation levels as well as a reduced design complexity, and silent operation (Heo *et al.* 2007; Cen & Erturk 2013). MFC bimorph actuation is a result of a distributed internal moment due to the contraction of two MFCs bonded by a layer of epoxy. We refer to this method of actuation as the internal actuation. While such smart materials are highly attractive for their use in biomimetic locomotion, previous research indicated that internally actuated propulsors underperform in terms of thrust and efficiency when compared to externally actuated propulsors (Yeh & Alexeev 2016*a*; Demirer *et al.* 2021). The deficiency of the internal actuation is linked to a suboptimal bending pattern of such propulsors with a characteristic cupping of the actuator tip increasing viscous losses. This therefore poses a question whether a hybrid actuation that uses a combination of external and internal actuation can yield superior hydrodynamics outperforming either of these actuation methods while offering a high degree of control over the bending pattern and propulsion characteristics.

In this work, we use fully coupled three dimensional simulations to probe the hydrodynamics of an elastic plate propulsor actuated at resonance by combined external and internal actuation representative of a heaving MFC bimorph. We examine the effects of a phase lag between the externally imposed heaving motion at the propulsor base and the internal distributed bending moment on the propulsor hydrodynamics. We consider hybrid propulsors in constrained and free swimming configurations. In the former configuration the plate is constrained from moving forward at its base, whereas in the later configuration the plate can swim freely. Our simulations indicate that the hybrid actuation results in a synergistic relationship between the internal and external actuation that drastically enhances the hydrodynamic performance of the plate propulsor.

2. Methodology

We consider a bio-inspired elastic propulsor with hybrid actuation that is driven by a combination of external and internal actuation to oscillate in an incompressible Newtonian fluid with density ρ and dynamic viscosity μ. The propulsor is represented by

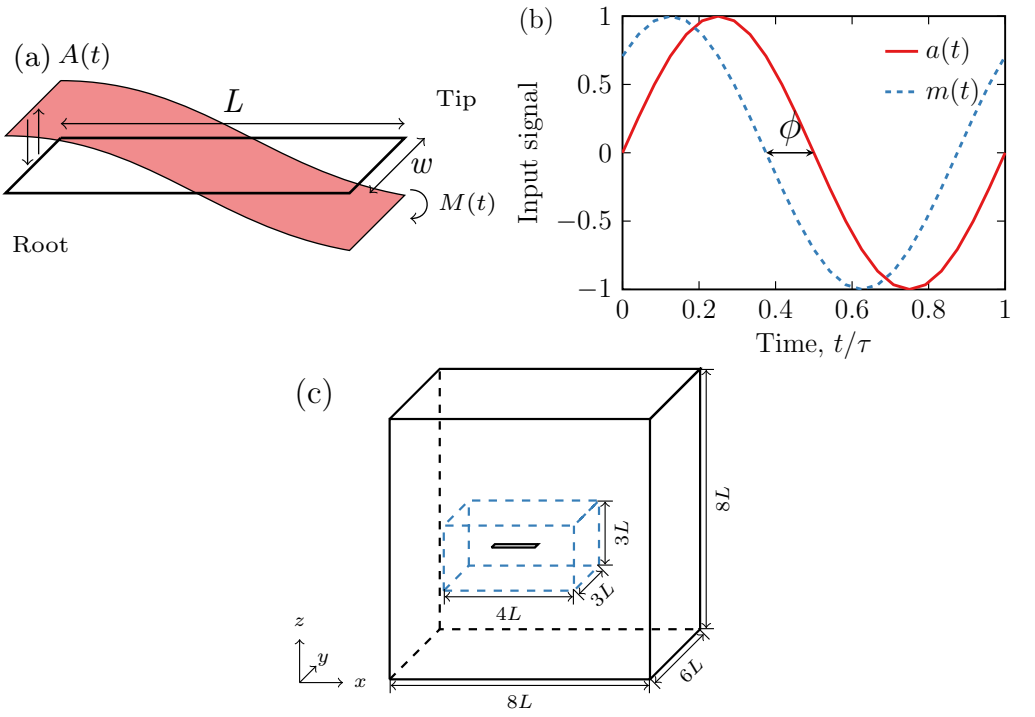

Figure 1: (a) Schematic of an oscillating elastic plate with length L, width w, and thickness $h \ll L$. The plate is actuated by a heaving motion at the base $a(t)$ and by a distributed internal bending moment $m(t)$. (b) Plate actuation signals with a phase lag ϕ. (c) Simulation domain consists of a coarse outer mesh and a fine inner mesh around the oscillating solid plate at the center.

a thin elastic plate of length L, width w, and thickness $h \ll L$, leading to an aspect ratio $\mathcal{A}_\mathcal{R} = L/w = 2.5$ (Figure 1a). The plate bending stiffness is D, the mass density is ρ_s, and the mass ratio is $\chi = \frac{\rho w}{\rho_s h} = 10$. The external actuation is imposed at the plate base leading to time-periodic heaving base oscillations $a(t) = A_0 L \sin(\omega t)$, where A_0 is the dimensionless heaving amplitude. The plate internal actuation is due to a time-periodic bending moment $m(t) = M_0 D \frac{L}{w} \sin(\omega t + \phi)$, where M_0 is the dimensionless moment amplitude and ϕ is the phase lag between the external and internal actuation. (Figure 1b). This time varying bending moment is imposed at the free end of the plate through a local force couple. Note that M_0 represents the magnitude of the static tip deflection of the plate due to the bending moment normalized by the plate length. Practically, the internal actuation represents the behavior of a macro-fiber composite (MFC) piezoelectric plate (Yeh & Alexeev 2016*a*; Demirer *et al.* 2021). Here, a local bending moment is generated by bonding two MFCs with a layer of epoxy and applying opposite currents to the two MFCs (Tan & Erturk 2018). Among different smart materials, MFCs strike an attractive balance between actuation and displacement levels as well as silent operation. The external and internal actuations share the same angular frequency $\omega = 2\pi/\tau$ with τ being the actuation period. We set $\omega = \omega_{res}$ with ω_{res} being the fundamental resonance frequency of the plate in fluid (Weaver Jr *et al.* 1990) leading to a Reynolds number $Re = \frac{\rho u_c L}{\mu} = 1000$, where $u_c = L/\tau$ the characteristic velocity. The corresponding plate stiffness D leads to the Cauchy number $C_y = \rho u_c^2 L^3/D = 0.065$ that relates the fluid

Table 1: Swimming characteristics of the reference externally actuated elastic plate with $A_0 = 0.1$.

Metric	Constrained	Free swimming
Propulsion	$F_r = 0.221$	$U_r = 0.6$
Power	$\mathcal{P}_r = 1.276$	$\mathcal{P}_r = 1.136$
Efficiency	$\eta_{r,c} = 0.173$	$\eta_{r,f} = 0.715$

loading to the plate elasticity. To explore the hydrodynamics of combined actuation, we fix the external actuation amplitude $A_0 = 0.1$ while varying the internal moment amplitude M_0 and the phase lag ϕ.

In the constrained configuration, the plate oscillates in a quiescent fluid and its base is kept in place in the x–direction (Figure 1c). The hydrodynamics of the constrained plate is characterized in terms of the dimensionless period-averaged thrust $F_x = f_x/f_c$, power $\mathcal{P} = p/p_c$, and efficiency $\eta_c = f_x u_c/p$. Here, $f_c = \frac{1}{2}\rho u_c^2 wL$ is the characteristic force, and $p_c = f_c u_c$ is the characteristic power. The instantaneous power is computed by integrating over the plate surface the dot product of the hydrodynamic forces and the local velocity. In the free swimming configuration, the plate is free to propel through the fluid in the x–direction. In this configuration the total drag and thrust acting on the plate balance each other leading to a net zero period-averaged hydrodynamic force. The free swimming is characterized by the dimensionless period-averaged swimming velocity $U = u/u_c$, power $\mathcal{P} = p/p_c$, and efficiency $\eta_f = uf_c/p$.

To characterize and compare the performance of propulsors with different actuation methods, we use an externally actuated plate at resonance with $A_0 = 0.1$ as a reference configuration. The characteristics of constrained and free swimming propulsors are normalized by the respective values for the constrained and free swimming reference propulsors. Table 1 provides the values of the relevant hydrodynamic characteristics for the reference propulsor configurations.

We model plate oscillations in a viscous fluid using a fully coupled fluid-structure interaction framework integrating a lattice Boltzmann (LB) model and a finite differences (FD) model (Demirer *et al.* 2021). The computational domain is fitted with a cubic lattice of equally spaced nodes with higher grid density near the oscillating plate as shown in Figure 1c. The flow is characterized by a velocity distribution function $g_i(\vec{r}, t)$ representing the density of fluid at position $\vec{r}$ that is propagating along the lattice direction i with velocity $\vec{c}$ at time t. We use a D3Q19 lattice that maintains 19 velocity directions in the three-dimensional space. We integrate the discrete Boltzmann equation to calculate the time evolution of the distribution function $g_i(\vec{r}, t)$ and retrieve relevant macroscopic quantities by taking moments of the distribution function (Ladd & Verberg 2001).

We set $\rho = 1$, $\mu = 1.25 \times 10^{-3}$, and $\tau = 2000$ in LB units. The fine and coarse fluid grids, respectively, measure $4L \times 3L \times 3L$ and $8L \times 6L \times 8L$, where $L = 50$ LB units. The fine and coarse node spacing are, respectively, $\Delta_f = 1$ and $\Delta_c = 2$ in LB units. The plate is discretized with 21 nodes in the length and 11 nodes in the width resulting in $\Delta_x = 2.381$ and $\Delta_y = 1.82$ in LB units. Further detail and validation of our computational framework can be found elsewhere (Masoud & Alexeev 2010, 2012; Mao & Alexeev 2014; Yeh & Alexeev 2014; Yeh *et al.* 2017, 2019; Demirer *et al.* 2021).

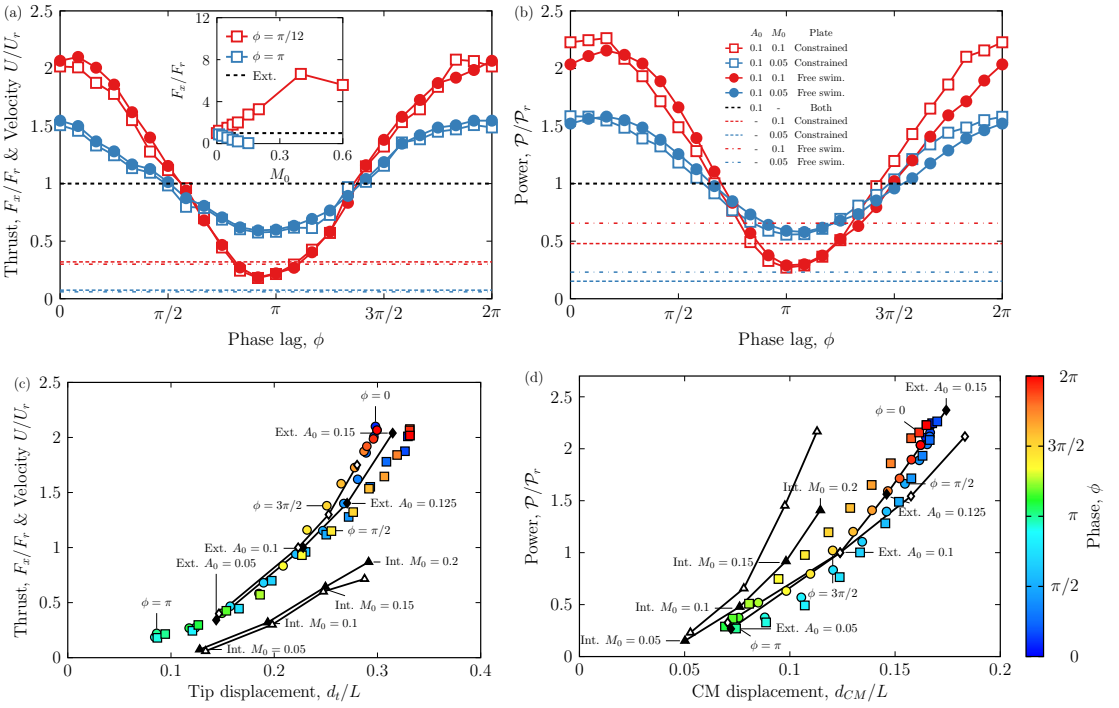

Figure 2: (a) Normalized thrust F_x/F_r and velocity U/U_r as a function of the phase difference between the internal and external actuation ϕ. The inset shows the maximum and minimum values of F_x/F_r as a function of M_0. (b) Normalized power $\mathcal{P}/\mathcal{P}_r$ as a function of ϕ. The horizontal dashed lines in (a) and (b) show the propulsion for internally actuated plates with $M_0 = 0.1$ (the red lines) and $M_0 = 0.05$ (the blue lines). The dashed lines show the thrust while the dash-dotted lines show the velocity. (c) Dependence of the thrust F_x and velocity U on the amplitude of the tip displacement d_t for $M_0 = 0.1$. (d) Dependence of the power $\mathcal{P}$ on the amplitude of the plate center of mass displacement d_{CM} for $M_0 = 0.1$. In (c) and (d), the colored circles and squares show, respective, the combined actuation data for free swimming and constrained configurations with the colors indicating the phase lag ϕ. The solid lines with symbols in (c) and (d) show the constrained external (the filled diamonds), free swimming external (the empty diamonds), constrained internal (the filled triangles), and free swimming internal (the empty triangles) actuation methods with different amplitudes of A_0 and M_0.

3. Results and discussion

Figure 2a shows the variation of the normalized thrust F_x/F_r for the constrained plate and the normalized swimming velocity U/U_r for the free swimming plate with the phase ϕ. We find that these two propulsion metrics are strongly correlated indicating that either can be used to characterize the plate propulsion. This correlation suggests that, with relation to their respective reference configurations (the constrained and free swimming externally actuated plates), the hybrid actuation dependence on ϕ is similarly proportional for the thrust and swimming velocity. The propulsion is maximized when the external actuation and the internal actuation are nearly in phase at $\phi = \pi/12$, and is minimized when the actuation signals are in phase opposition about $\phi = 11\pi/12$. Compared to the externally actuated reference case, the combined actuation with $M_0 =$

0.1 doubles the propulsion, whereas using $M_0 = 0.05$ increases the propulsion by about 50%. The propulsion with combined actuation increases to nearly 7.7 times of the reference case with $M_0 = 0.4$ (see the inset in Figure 2a). For $M_0 > 0.4$ the free end cupping negatively affects the swimming performance of combined actuation decreasing the propulsion. When the plate is actuated out of phase the combined actuation can reduce the propulsion to nearly zero. Note that the propulsion is not symmetric with respect to $\phi = 0$ or $\phi = \pi$. At $\phi = \pi/2$, $F_x/F_r \simeq 1$, while at $\phi = 3\pi/2$, $F_x/F_r \simeq 1.28$ leading to a 28% difference. Note also that the internal actuation alone with, respectively, $M_0 = 0.1$ and $M_0 = 0.05$ yields propulsion that is only about 50% and 10% of that of the externally actuated plate. Thus, the combined actuation not only enables wide control over the propulsion, but can yield propulsion that significantly exceeds the sum of the propulsion of the plates with separate external and internal types of actuation.

As shown in Figure 2b the power exhibits a dependence on ϕ that is similar to that of the propulsion. The power is maximized at $\phi = \pi/6$ and minimized at $\phi = \pi$. The maximum power of the plate with combined actuation significantly exceeds the cumulative power of plates with separate external and internal actuation. Furthermore, the combined actuation can greatly reduce $\mathcal{P}$ compared to the externally actuated plate. Similarly to the propulsion, the power is not symmetric with respect to $\phi = 0$ or $\phi = \pi$. At $\phi = \pi/2$, $\mathcal{P}/\mathcal{P}_r \simeq 1.49$, while at $\phi = 3\pi/2$, $\mathcal{P}/\mathcal{P}_r \simeq 1.2$ which corresponds to a nearly 20% difference in power. We attribute this symmetry breaking to non-linear effects arising due to the large deformation of the plate actuated with the hybrid actuation method.

The trailing edge displacement d_t is a major parameter that controls the plate propulsion (Michelin & Llewellyn Smith 2009). Figure 2c shows the propulsion metrics as a function of d_t (see Supplementary Information Figure S1 for the dependence of d_t on ϕ). We find that there is a direct relationship between the velocity and thrust data and the trailing edge displacement. The data for externally actuated plates with varying actuation amplitudes in the free swimming and constrained configurations closely match the results for the propulsors with combined actuation. On the contrary, free swimming and constrained internally actuated plates with varying M_0 yield significantly lower performance than the combined actuation for comparable tip displacement. This is consistent with previous results (Demirer *et al.* 2021) and can be attributed to the sub-optimal bending pattern of internally actuated plates. Thus, in the case of combined actuation the phase ϕ controls the tip displacement which, in turn, defines the propulsion characteristics. Note that with the combined and external actuation methods, U/U_r in the free swimming configuration increases slightly faster than F_x/F_r in the constrained configuration with increasing d_t. Furthermore, the free swimming configuration results in somewhat smaller d_t compared to the constrained configuration, which is related to an increased added mass effect due to the incoming fluid flow.

As shown in Figure 2d, the power $\mathcal{P}$ scales with the displacement of the plate center of mass d_{CM} (see Supplementary Information Figure S1 for the dependence of d_{CM} on ϕ). The power consumption is minimized with the reduced center of mass (CM) displacement and gradually increases with increasing d_{CM}. The plates with the combined actuation and the external actuation show similar dependencies, whereas the internally actuated plate requires a slightly greater power for the same CM deflection. Note that d_t and d_{CM} for the plates with combined actuation are maximized when the external and internal actuation act in phase $\phi = \pi/12$ and minimized when they are in phase opposition $\phi = \pi$.

In Figure 3a we show the efficiencies η_c and η_f for, respectively, constrained and free swimming plates with combined actuation. Both these parameters reveal a similar dependence on ϕ. More importantly, the efficiency can significantly exceed the value characterizing the plate with the external actuation. The maximum efficiency of the

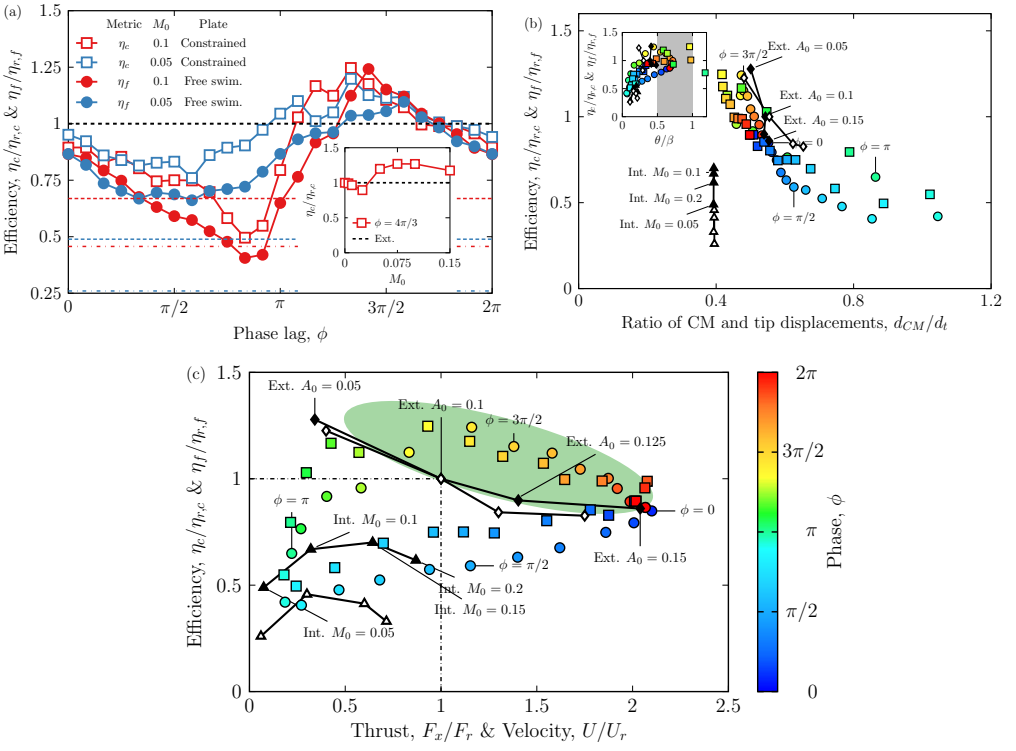

Figure 3: (a) Normalized constrained efficiency $\eta_c/\eta_{c,r}$ and free swimming efficiency $\eta_f/\eta_{f,r}$ as a function of the phase difference ϕ. The inset shows the maximum efficiency as a function of M_0. The horizontal lines show the efficiency for internally actuated plates with $M_0 = 0.1$ (the red lines) and $M_0 = 0.05$ (the blue lines). (b) Dependence of the efficiencies η_c and η_f on the ratio between the center of mass and tip deflections d_{CM}/d_t for $M_0 = 0.1$. The inset show the efficiency as a function of θ/β. (c) Dependence of the efficiencies η_c and η_f on the thrust F_x and velocity U for $M_0 = 0.1$. In (b) and (c), the colored circles and squares show, respective, the combined actuation data for free swimming and constrained configurations with the colors indicating the phase lag ϕ. The solid lines with symbols in (b) and (c) show the constrained external (the filled diamonds), free swimming external (the empty diamonds), constrained internal (the filled triangles), and free swimming internal (the empty triangles) actuation methods with different amplitudes of A_0 and M_0.

combined actuation is about 25% greater than that of the externally actuated plate. The phase difference $\phi = 4\pi/3$ leading to this actuation regime is nearly independent of M_0. The enhancement of the efficiency is maximized when $M_0 \simeq 0.075$ as shown in the inset in Figure 3a. When $M_0 < 0.04$, the efficiency decreases below the reference value. In this M_0 range, the increased power due to the internal actuation outweighs its benefit for the propulsion. For greater M_0, the internal actuation translates into a significant increase of the plate efficiency up to $M_0 \simeq 0.1$. Further increase of M_0 yields a less efficient propulsion due to the tip cupping.

Note that the phase of the maximum thrust and the maximum velocity $\phi = \pi/12$ does not match the phase of the maximum efficiency $\phi = 4\pi/3$. Thus, the maximum propulsion is achieved at the cost of reduced efficiency. Furthermore, the combined actuation with

$M_0 = 0.4$ that yields the overall maximum thrust $F_x/F_r \simeq 7.7$ at $\phi = \pi/12$ (Figure 2a) has an efficiency reduced to $\eta_c/\eta_{r,c} \simeq 0.86$ whereas at $\phi = 4\pi/3$ the thrust is $F_x/F_r \simeq 2$ and the efficiency is $\eta_c/\eta_{r,c} \simeq 0.98$.

The efficiency represents the ratio of the propulsion metrics and the power. Since the propulsion and the power scale with, respectively, d_t and d_{CM}, in Figure 3b we plot η_c and η_f as a function of d_{CM}/d_t. Indeed we find that the data for the plates with combined actuation clusters closely showing a decreasing trend with increasing d_{CM}/d_t. Thus, for an efficient propulsion the bending pattern needs to have low d_{CM} and high d_t, whereas plate oscillations in which d_{CM} increases with respect to d_t result in less efficient propulsion. For plates with independent internal and external actuation, we find that d_{CM}/d_t changes only slightly with the amplitude since at resonance the bending patterns weakly depend on the oscillation amplitude.

Note that for the plates with internal actuation only, d_{CM}/d_t is relatively small compared to externally actuated plates and about the same value as the lowest d_{CM}/d_t obtained with the hybrid actuation. Nevertheless, these propulsors show a low efficiency due to the suboptimal tip bending. Thus, having low d_{CM}/d_t is insufficient for efficient locomotion. In the inset in Figure 3b, we show the efficiency as a function of the ratio θ/β between the tip angle at the maximum velocity θ and the base angle $\beta = \arctan \frac{\omega A_0 L}{U}$ (Ramananarivo *et al.* 2011) (see Supplementary Information Figure S2). In the constrained configuration, the plate oscillates in quiescent fluid, therefore we approximate the cruising velocity U by the tip velocity V_t leading to $\beta = \arctan \frac{\omega A_0 L}{V_t}$. For efficient swimming, θ/β should be in the range between 0.5 and 1 (Ramananarivo *et al.* 2011). We find that the externally actuated plates and the plates with hybrid actuation with higher efficiency are indeed close to the range of efficient θ/β. The internally actuated plates, on the other hand, have θ/β that are much lower than the optimum range confirming that the low efficiency is due to the bending pattern with a suboptimum tip angle.

Overall, the propulsor performance is enhanced when both the efficiency and propulsion are maximized. In Figure 3c we show the relationship between the efficiency and the propulsion. For the plate with the external actuation, the efficiency decreases with increasing propulsion. Thus, one needs to compromise with either having a propulsor that maximizes its efficiency or propulsion. Although the internally actuated plate performs poorly compared to the plate with the external actuation, the plate with a combination of the external and internal actuation yields a propulsors that significantly outperforms the externally actuated plate by both characteristics simultaneously, as indicated by the green ellipse in Figure 3c. The combined actuation exceeds the externally actuated propulsor for both the propulsion and efficiency in a wide range of $3\pi/2 < \phi < 2\pi$. Note that the maximum propulsion at $\phi = \pi/12$ is characterized by higher efficiency than an equivalent propulsion level achieved by the external actuation with an increased actuation amplitude. The combined actuation yields up to 60% greater propulsion for the same efficiency and is 25% more efficient for the same propulsion output compared to the plate with the external actuation.

In Figure 4, we examine the bending pattern and the hydrodynamics of plates with combined actuation at the maximum efficiency ($\phi = 4\pi/3$) and the maximum propulsion ($\phi = \pi/12$) (see also Supplementary Information Figure S3 for additional ϕ). At the maximum propulsion the palate exhibits a typical bending pattern for actuation at resonance that maximizes the tip deflection (Figure 4a). At the maximum efficiency the bending pattern develops a dip near the middle of the plate reducing the displacement of the center of mass (Figure 4b). Note that the bending pattern at $\phi = \pi/12$ is similar to that of an externally actuated plate, whereas the internally actuated plate shows a

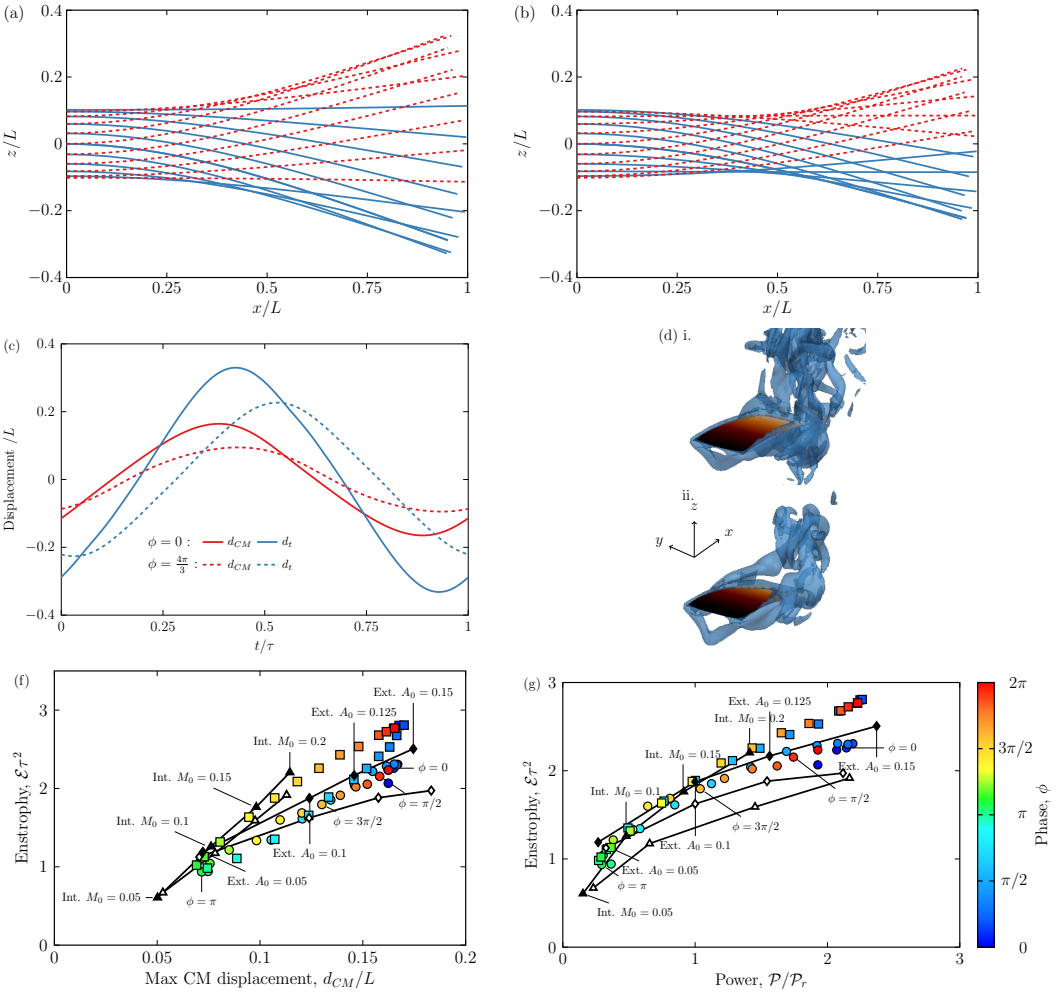

Figure 4: (a) Bending pattern of a plate with combined actuation at the maximum thrust ($\phi = \pi/12$). (b) Bending pattern of a plate with combined actuation at the maximum efficiency ($\phi = 4\pi/3$). The solid blue lines and the dashed red lines in (a) and (b) correspond to the plate profiles during, respectively, the upstroke and downstroke. (c) Time histories of the tip displacement d_t and the center of mass displacement d_{CM} at the maximum efficiency and the maximum thrust. (d) Contours of the normalized vorticity $\omega\tau = 10$ for (i) the maximum thrust and (ii) the maximum efficiency, see supplementary Video S1. (f) Dependence of the enstrophy $\mathcal{E}$ on the center of mass maximum displacement d_{CM}. (g) Dependence of the enstrophy $\mathcal{E}$ on the power $\mathcal{P}$. In (f) and (g), the colored circles and squares show, respective, the combined actuation data for free swimming and constrained configurations with the colors indicating the phase lag ϕ. The solid lines with symbols in (f) and (g) show the constrained external (the filled diamonds), free swimming external (the empty diamonds), constrained internal (the filled triangles) and free swimming internal (the empty triangles) actuation with different amplitudes of A_0 and M_0.

distinctly different pattern with no displacement at the root and non-vanishing curvature at the tip (Demirer *et al.* 2021) (see Supplementary Information Figure S4).

The tip and CM displacements over an oscillation period are shown in Figure 4c. At $\phi = \pi/12$, the tip and CM move by nearly 50% more than at $\phi = 4\pi/3$. In terms of the phase lag between the tip and actuation signals φ, our simulations show that in the regime of the maximum efficiency the tip and actuation are in phase quadrature that is characteristic of resonance oscillations, whereas at the maximum efficiency the phase is $\varphi \simeq 2\pi/3$. This confirms that the combined actuation modulates φ and, therefore, the bending mode (see Supplementary Information Figure S5).

We use the mean enstrophy $\mathcal{E}$ to quantify the vorticity generated by the plates (Demirer *et al.* 2021). We find that $\mathcal{E}$ roughly scales with d_{CM} (Figure 4e), indicating that the magnitude of CM displacement dictates to a large extent the amount of vorticity produced by the plate. The plates with solely internal and external actuations generate $\mathcal{E}$ similar to that of the combined actuation plate. Furthermore, when $\mathcal{E}$ is plotted against the power $\mathcal{P}$ (Figure 4f), we find that the data for all actuation methods collapse into a single curve. Thus, the power indeed scales with the amount of enstrophy, which in turn is defined by the center of mass displacement. Interestingly, the enstrophy is sensitive to the plate configuration. Free swimming plates generate significantly less enstrophy than constrained plates for comparable power $\mathcal{P}$, when $\mathcal{P}$ is sufficiently large. This holds for combined, external, and internal actuation methods.

4. Conclusions

We show that the hybrid internal-external actuation can be used to regulate the hydrodynamic performance of a propulsor by changing the phase difference between the actuation methods while maintaining high efficiency outperforming propulsors with a single actuation method. Our results suggest that the propulsion scales with the magnitude of the tip displacement, whereas the power scales with the displacement of the center of mass of the propulsor. The hybrid actuation provides a unique way to regulate the balance between these two metrics, thereby yielding an efficient propulsor with superior performance. These findings indicate that energy dissipation is mostly associated with the vortex generation and side edge vortices, whereas the propulsion is controlled by the trailing edge vortices consistently with previous studies on flexible propulsors (Raspa *et al.* 2014; Yeh & Alexeev 2016*b*; Quinn *et al.* 2014; Dai *et al.* 2012; Li *et al.* 2017). The hybrid propulsor performance is analyzed in the constrained configuration, where the propulsor oscillates in a quiescent fluid and its base is kept from moving forward, and in the free swimming configurations, where the propulsor can freely propel forward through the fluid. Our simulations show that the hydrodynamic performance in these two configurations is closely correlated, although in free swimming, the propulsor exhibits a slightly lower trailing edge displacement due to the effect of upcoming fluid flow.

Our results are also useful for developing biomimetic propulsors with other modes of combined actuation, such as propulsors using a combination of heaving and pitching root actuation. Such propulsors are the subject of numerous studies indicating that the angle of attack and the phase lag between the heaving and pitching are critical parameters to maximize the efficiency (Piñeirua *et al.* 2017; Smits 2019; Quinn *et al.* 2015). In particular, it is shown that the thrust is maximized at the phase difference $11\pi/6$, the power is minimized at $7\pi/6$, and the efficiency is maximized at $3\pi/2$ (Van Buren *et al.* 2019), which are close to the respective phases identified for the hybrid internal-external actuation.

Macro fiber composite (MFC) piezoelectric materials are particularly attractive for designing active propulsors with combined actuation due to their robustness and high efficiency (Sodano 2003; Williams *et al.* 2006; Cen & Erturk 2013). In this case, the base of the MFC propulsor can be actuated using a mechanical system similar to those used in current designs (Mason & Burdick 2000; Yan *et al.* 2008; Wu *et al.* 2015), whereas the piezoelectric actuation can be harnessed to impose a time-periodic internal bending moment dynamically modulating the propulsor shape. The use of active propulsors, such as made of MFC piezoelectric materials, is especially promising for designing small scale robotic swimmers due to the reduced mechanical complexity, the ease of integration, and operational control of such propulsors (Tan & Erturk 2018). We note that our simulations point to the superior hydrodynamic efficiency of the propulsors with combined actuation. In practice, additional energy losses associated with the driving and control mechanisms need to be accounted for evaluating the overall swimmer performance. While it depends on specific implementation, piezoelectric materials typically exhibit high efficiency, up to 90%, in converting electrical energy into mechanical work (Richards *et al.* 2004; Steiger & Mokrỳ 2015; Nabawy & Crowther 2016). As such, it can be expected that MFC propulsors can yield high overall efficiency compared to traditional mechanical propulsors, while benefiting from the reduced size, enhanced robustness, and operational flexibility.

The performing of propulsors with combined actuation can potentially be further improved by employing more advanced forms of internal actuation, such as segmented MFC actuators with independent control of individual sequential segments. In this scenario, each segment can be used to impose a bending moment enabling greater control over the dynamics of the propulsor that can be further optimized to mimic fish-like kinematics for enhanced hydrodynamic performance. Furthermore, the hybrid propulsors can be used not only for forward propulsion, but also for swimmer navigation by applying asymmetric actuation to the MFCs simplifying the robotic swimmer design and operation. Finally, piezoelectric propulsors can be used to harvest energy from the unsteady fluid environment enabling increased autonomy of the robotic swimmer (Yang *et al.* 2009; Erturk & Inman 2011; Song *et al.* 2010).

5. Acknowledgments

We thank the National Science Foundation (CBET-1705739) for financial support.

REFERENCES

Alben, Silas, Witt, Charles, Baker, T Vernon, Anderson, Erik & Lauder, George V 2012 Dynamics of freely swimming flexible foils. *Physics of Fluids* **24** (5), 051901.

Anderson, JM, Streitlien, K, Barrett, DS & Triantafyllou, MS 1998 Oscillating foils of high propulsive efficiency .

Cen, L & Erturk, A 2013 Bio-inspired aquatic robotics by untethered piezohydroelastic actuation. *Bioinspiration & Biomimetics* **8** (1), 016006.

Chen, Zheng, Shatara, Stephan & Tan, Xiaobo 2009 Modeling of biomimetic robotic fish propelled by an ionic polymer–metal composite caudal fin. *IEEE/ASME transactions on mechatronics* **15** (3), 448–459.

Chen, Zheng, Um, Tae I, Zhu, Jianzhong & Bart-Smith, Hilary 2011 Bio-inspired robotic cownose ray propelled by electroactive polymer pectoral fin. In *ASME 2011 international mechanical engineering congress and exposition*, pp. 817–824. American Society of Mechanical Engineers Digital Collection.

Chu, Won-Shik, Lee, Kyung-Tae, Song, Sung-Hyuk, Han, Min-Woo, Lee, Jang-Yeob, Kim, Hyung-Soo, Kim, Min-Soo, Park, Yong-Jai, Cho, Kyu-Jin & Ahn, Sung-

Hoon 2012 Review of biomimetic underwater robots using smart actuators. *International journal of precision engineering and manufacturing* **13** (7), 1281–1292.

Combes, S. A. & Daniel, T. L. 2001 Shape, flapping and flexion: wing and fin design for forward flight. *Journal of Experimental Biology* **204** (12), 2073–2085, arXiv: https://jeb.biologists.org/content/204/12/2073.full.pdf.

Dai, Hu, Luo, Haoxiang, de Sousa, Paulo JSA Ferreira & Doyle, James F 2012 Thrust performance of a flexible low-aspect-ratio pitching plate. *Physics of Fluids* **24** (10), 101903.

Demirer, Ersan, Wang, Yu-Cheng, Erturk, Alper & Alexeev, Alexander 2021 Effect of actuation method on hydrodynamics of elastic plates oscillating at resonance. *Journal of Fluid Mechanics* **910**.

Erturk, Alper & Inman, Daniel J 2011 *Piezoelectric energy harvesting*. John Wiley & Sons.

Esposito, Christopher J., Tangorra, James L., Flammang, Brooke E. & Lauder, George V. 2012 A robotic fish caudal fin: effects of stiffness and motor program on locomotor performance. *Journal of Experimental Biology* **215** (1), 56–67, arXiv: https://jeb.biologists.org/content/215/1/56.full.pdf.

Fish, FEandlauder & Lauder, George V 2006 Passive and active flow control by swimming fishes and mammals. *Annu. Rev. Fluid Mech.* **38**, 193–224.

Flammang, B. E. & Lauder, G. V. 2009 Caudal fin shape modulation and control during acceleration, braking and backing maneuvers in bluegill sunfish, lepomis macrochirus. *Journal of Experimental Biology* **212** (2), 277–286, arXiv: https://jeb.biologists.org/content/212/2/277.full.pdf.

Heo, Seok, Wiguna, Tedy, Park, Hoon Cheol & Goo, Nam Seo 2007 Effect of an artificial caudal fin on the performance of a biomimetic fish robot propelled by piezoelectric actuators. *Journal of Bionic Engineering* **4** (3), 151–158.

Hoover, Alexander P, Cortez, Ricardo, Tytell, Eric D & Fauci, Lisa J 2018 Swimming performance, resonance and shape evolution in heaving flexible panels. *Journal of Fluid Mechanics* **847**, 386–416.

Hu, H., Liu, J., Dukes, I. & Francis, G. 2006 Design of 3d swim patterns for autonomous robotic fish. In *2006 IEEE/RSJ International Conference on Intelligent Robots and Systems*, pp. 2406–2411.

Jayne, Bruce C & Lauder, GEORGE V 1995 Speed effects on midline kinematics during steady undulatory swimming of largemouth bass, micropterus salmoides. *Journal of Experimental Biology* **198** (2), 585–602.

Kolomenskiy, D., Moffatt, H. K., Farge, M. & Schneider, K. 2011 The lighthill–weis-fogh clap–fling–sweep mechanism revisited. *Journal of Fluid Mechanics* **676**, 572–606.

Kopman, V., Laut, J., Acquaviva, F., Rizzo, A. & Porfiri, M. 2015 Dynamic modeling of a robotic fish propelled by a compliant tail. *IEEE Journal of Oceanic Engineering* **40** (1), 209–221.

Ladd, AJC & Verberg, R 2001 Lattice-boltzmann simulations of particle-fluid suspensions. *Journal of statistical physics* **104** (5-6), 1191–1251.

Lauder, George V. & Tangorra, James L. 2015 *Fish Locomotion: Biology and Robotics of Body and Fin-Based Movements*, pp. 25–49. Berlin, Heidelberg: Springer Berlin Heidelberg.

Lauder, George V & Tytell, Eric D 2005 Hydrodynamics of undulatory propulsion. *Fish physiology* **23**, 425–468.

Li, Ningyu, Liu, Huanxing & Su, Yumin 2017 Numerical study on the hydrodynamics of thunniform bio-inspired swimming under self-propulsion. *PloS one* **12** (3), e0174740.

Liu, H & Aono, Hikaru 2009 Size effects on insect hovering aerodynamics: an integrated computational study. *Bioinspiration & Biomimetics* **4** (1), 015002.

Mao, Wenbin & Alexeev, Alexander 2014 Motion of spheroid particles in shear flow with inertia. *Journal of Fluid Mechanics* **749**, 145–166.

Marras, Stefano & Porfiri, Maurizio 2012 Fish and robots swimming together: attraction towards the robot demands biomimetic locomotion. *Journal of The Royal Society Interface* **9** (73), 1856–1868.

Mason, Richard & Burdick, Joel W 2000 Experiments in carangiform robotic fish locomotion. In *Proceedings 2000 ICRA. Millennium Conference. IEEE International*

Conference on Robotics and Automation. Symposia Proceedings (Cat. No. 00CH37065), , vol. 1, pp. 428–435. IEEE.

Masoud, Hassan & Alexeev, Alexander 2010 Resonance of flexible flapping wings at low reynolds number. *Physical Review E* **81** (5), 056304.

Masoud, Hassan & Alexeev, Alexander 2012 Efficient flapping flight using flexible wings oscillating at resonance. In *Natural Locomotion in Fluids and on Surfaces*, pp. 235–245. Springer.

McHenry, Matthew J, Pell, Charles A & Long, JH 1995 Mechanical control of swimming speed: stiffness and axial wave form in undulating fish models. *Journal of Experimental Biology* **198** (11), 2293–2305.

Michelin, Sébastien & Llewellyn Smith, Stefan G 2009 Resonance and propulsion performance of a heaving flexible wing. *Physics of Fluids* **21** (7), 071902.

Nabawy, Mostafa RA & Crowther, William J 2016 Dynamic electromechanical coupling of piezoelectric bending actuators. *Micromachines* **7** (1), 12.

Pabst, D. Ann 2015 Springs in Swimming Animals. *American Zoologist* **36** (6), 723–735, arXiv: https://academic.oup.com/icb/article-pdf/36/6/723/733033/36-6-723.pdf.

Philen, Michael & Neu, Wayne 2011 Hydrodynamic analysis, performance assessment, and actuator design of a flexible tail propulsor in an artificial alligator. *Smart Materials and Structures* **20** (9), 094015.

Piñeirua, Miguel, Thiria, Benjamin & Godoy-Diana, Ramiro 2017 Modelling of an actuated elastic swimmer. *arXiv preprint arXiv:1712.08463* .

Quinn, Daniel B, Lauder, George V & Smits, Alexander J 2014 Scaling the propulsive performance of heaving flexible panels. *Journal of fluid mechanics* **738**, 250–267.

Quinn, Daniel B., Lauder, George V. & Smits, Alexander J. 2015 Maximizing the efficiency of a flexible propulsor using experimental optimization. *Journal of Fluid Mechanics* **767**, 430–448.

Ramananarivo, Sophie, Godoy-Diana, Ramiro & Thiria, Benjamin 2011 Rather than resonance, flapping wing flyers may play on aerodynamics to improve performance. *Proceedings of the National Academy of Sciences* **108** (15), 5964–5969, arXiv: https://www.pnas.org/content/108/15/5964.full.pdf.

Ramananarivo, Sophie, Godoy-Diana, Ramiro & Thiria, Benjamin 2013 Passive elastic mechanism to mimic fish-muscle action in anguilliform swimming. *Journal of The Royal Society Interface* **10** (88), 20130667.

Raspa, V, Ramananarivo, S, Thiria, B & Godoy-Diana, R 2014 Vortex-induced drag and the role of aspect ratio in undulatory swimmers. *Physics of Fluids* **26** (4), 041701.

Richards, Cecilia D, Anderson, Michael J, Bahr, David F & Richards, Robert F 2004 Efficiency of energy conversion for devices containing a piezoelectric component. *Journal of Micromechanics and Microengineering* **14** (5), 717.

Smits, Alexander J 2019 Undulatory and oscillatory swimming. *Journal of Fluid Mechanics* **874**.

Sodano, Henry Angelo 2003 Macro-fiber composites for sensing, actuation and power generation. PhD thesis, Virginia Tech.

Song, Hyun Jeong, Choi, Young-Tai, Wereley, Norman M & Purekar, Ashish S 2010 Energy harvesting devices using macro-fiber composite materials. *Journal of Intelligent Material Systems and Structures* **21** (6), 647–658.

Steiger, Kateřina & Mokrỳ, Pavel 2015 Finite element analysis of the macro fiber composite actuator: macroscopic elastic and piezoelectric properties and active control thereof by means of negative capacitance shunt circuit. *Smart Materials and Structures* **24** (2), 025026.

Su, Z., Yu, J., Tan, M. & Zhang, J. 2014 Implementing flexible and fast turning maneuvers of a multijoint robotic fish. *IEEE/ASME Transactions on Mechatronics* **19** (1), 329–338.

Tan, D & Erturk, A 2018 On the coupling of nonlinear macro-fiber composite piezoelectric cantilever dynamics with hydrodynamic loads. In *Active and Passive Smart Structures and Integrated Systems XII*, , vol. 10595, p. 105950R. International Society for Optics and Photonics.

Triantafyllou, Michael S & Triantafyllou, George S 1995 An efficient swimming machine. *Scientific american* **272** (3), 64–70.

Van Buren, Tyler, Floryan, Daniel & Smits, Alexander J 2019 Scaling and performance of simultaneously heaving and pitching foils. *AIAA Journal* **57** (9), 3666–3677.

Wang, Zhenlong, Hang, Guanrong, Li, Jian, Wang, Yangwei & Xiao, Kai 2008 A micro-robot fish with embedded sma wire actuated flexible biomimetic fin. *Sensors and Actuators A: Physical* **144** (2), 354–360.

Wardle, CSJJ, Videler, John & Altringham, J 1995 Tuning in to fish swimming waves: body form, swimming mode and muscle function. *Journal of experimental Biology* **198** (8), 1629–1636.

Weaver Jr, William, Timoshenko, Stephen P & Young, Donovan Harold 1990 *Vibration problems in engineering*. John Wiley & Sons.

Williams, R Brett, Inman, Daniel J & Wilkie, W Keats 2006 Nonlinear response of the macro fiber composite actuator to monotonically increasing excitation voltage. *Journal of Intelligent Material Systems and Structures* **17** (7), 601–608.

Wu, ZhengXing, Yu, JunZhi, Su, ZongShuai, Tan, Min & Li, ZhenLong 2015 Towards an esox lucius inspired multimodal robotic fish. *Science China Information Sciences* **58** (5), 1–13.

Yan, Qin, Han, Zhen, Zhang, Shi-wu & Yang, Jie 2008 Parametric research of experiments on a carangiform robotic fish. *Journal of Bionic Engineering* **5** (2), 95–101.

Yang, Yaowen, Tang, Lihua & Li, Hongyun 2009 Vibration energy harvesting using macro-fiber composites. *Smart materials and structures* **18** (11), 115025.

Yeh, Peter Derek & Alexeev, Alexander 2014 Free swimming of an elastic plate plunging at low reynolds number. *Physics of Fluids* **26** (5), 053604.

Yeh, Peter D & Alexeev, Alexander 2016*a* Biomimetic flexible plate actuators are faster and more efficient with a passive attachment. *Acta Mechanica Sinica* **32** (6), 1001–1011.

Yeh, Peter Derek & Alexeev, Alexander 2016*b* Effect of aspect ratio in free-swimming plunging flexible plates. *Computers & Fluids* **124**, 220–225.

Yeh, Peter D., Demirer, Ersan & Alexeev, Alexander 2019 Turning strategies for plunging elastic plate propulsor. *Phys. Rev. Fluids* **4**, 064101.

Yeh, Peter D., Li, Yuanda & Alexeev, Alexander 2017 Efficient swimming using flexible fins with tapered thickness. *Phys. Rev. Fluids* **2**, 102101.

Yu, Junzhi, Tan, Min, Wang, Shuo & Chen, Erkui 2004 Development of a biomimetic robotic fish and its control algorithm. *IEEE Transactions on Systems, Man, and Cybernetics, Part B (Cybernetics)* **34** (4), 1798–1810.